Catalysis under microscope: Unraveling the mechanism of catalyst de- and re-activation in the continuous dimethyl carbonate synthesis from CO_2 and methanol in the presence of a dehydrating agent

Dragos Stoian[1, 2], Atul Bansode[1], Francesc Medina[2], Atsushi Urakawa[1*]

[1] Institute of Chemical Research of Catalonia (ICIQ), The Barcelona Institute of Science and Technology, Av. Països Catalans 16, 43007 Tarragona, Spain

[2] Department of Chemical Engineering, University Rovira i Virgili, Av. Països Catalans 26, 43007 Tarragona, Spain

Abstract

The high efficiency of 2-cyanopyridine (2-CP) as dehydrating agent in the direct dimethyl carbonate (DMC) synthesis from CO_2 and methanol over CeO_2 catalysts has been recently demonstrated with excellent DMC yields (>90%) in both batch and continuous operations. The catalytic reaction is expected to involve a complex three-phase boundary due to the high boiling points of 2-CP and also 2-picolinamide (2-PA) formed by hydration of 2-CP. The catalyst is also known to deactivate noticeably in the time-scale of days during the continuous operation. The aim of this work is to gain visual information of the catalyst under *operando* conditions by means of an optically transparent, fused quartz reactor to understand the behavior of catalyst deactivation and to learn about the phase behavior of the reaction mixture. The catalytic tests using the fused quartz reactor could reproduce the results observed in a common stainless steel reactor, and the effects of reaction temperature and pressure (up to 30 bar) were examined in detail to show that there is an optimum condition (30 bar, 120 °C) to

achieve the best catalytic performance. The visual inspection was further combined with IR and Raman spectroscopic studies to identify the origin of the catalyst deactivation and establish an efficient catalyst reactivation protocol. Interestingly, not coke but 2-PA surface adsorption was found responsible for the catalyst deactivation. The *operando* visual inspection evidenced that the surface of the CeO_2 catalyst particles is constantly wet and also coated with some crystallites (likely of 2-PA) during the reaction, whereas the bulk of the CeO_2 particle is still accessible for the reactants and thus available for the reaction.

Keywords: carbon dioxide, methanol, dimethyl carbonate, 2-cyanopyridine, *operando* study, continuous reaction, catalyst de-/re-activation.

1. Introduction

Human activities have been influencing climate to change by the significant increase in the emissions of greenhouse gases, among which carbon dioxide (CO_2) is the main exponent. According to Friedlingstein *et al*., human activities are responsible for 35 billion metric tons (gigatons) of CO_2 emission in 2010 [1], an amount that makes the CO_2 emissions from the world's degassing subaerial and submarine volcanoes seem rather small [2]. In this context, exploring new ways to valorize CO_2 in a form of chemicals such as fuel [3] and organic carbonates has gained great attention. Among them, development of the direct carboxylation reaction of alcohols such as methanol and ethanol with CO_2 for the synthesis of alkyl carbonates is attractive in terms of CO_2 chemical fixation and green chemistry (organic carbonates are well known for their low

toxicity, non-corrosivity and biodegradability) [4, 5]. Also, the reaction can contribute to the substitution of toxic phosgene by abundant and less harmful CO_2 molecule.

Dimethyl carbonate (DMC) has attracted much attention in the last few decades due to its unique chemical properties as a safe, non-corrosive and environmentally acceptable alternative to methylating and carbonylating agents (CH_3X, DMS, $COCl_2$) [4-8]. Also, DMC has been used in the synthesis of polycarbonates and polyurethane, and even as a solvent, replacing methyl ethyl ketone, butanone, or *tert*-butyl acetate [4, 9]. Moreover, due to its high oxygen content (around 53 wt%; three-times more oxygen-rich than methyl *tert*-butyl ether, MTBE), DMC has been employed as an oxygenate additive to diesel fuel, thus increasing the potential to reduce soot from diesel engines [10].

Both batch and continuous operations have been reported for the direct DMC synthesis using heterogeneous catalysts from carbon dioxide and methanol as a safer and cleaner way for DMC production, eliminating the use of the toxic phosgene or CO required for the conventional DMC synthesis. The reaction can, in principle, provide an extremely high atom efficiency (**Reaction 1**).

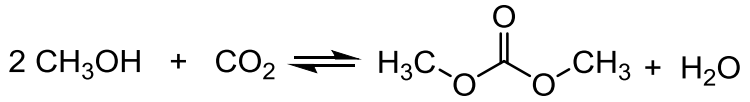

(1)

Zirconia and ceria are the catalyst materials widely reported for the methanol carboxylation reaction [11-20]. Even though the selectivity towards DMC (S_{DMC}) can be very high (almost 100% in some cases), the methanol conversion (X_{MeOH}) is limited by the reaction equilibrium. Attempts have been made with more complex vanadium-based catalysts such as H_3PO_4/V_2O_5 and Cu-Ni/V_2O_5-SiO_2 [21, 22], without improving the

methanol conversion and DMC yield to a large extent. Different oxides like SiO_2, Al_2O_3, TiO_2, H-ZSM-5, H-USY, H-MOR, ZnO, MoO_3, and Bi_2O_3 were tested in the reaction, but mainly dimethyl ether (DME) was produced instead of desired DMC [12].

Several researchers have examined different ways to improve the thermodynamically-limited equilibrium conversion to shift towards DMC formation, because DMC yield is <1% even at thermodynamically favorable high pressure conditions [23, 24]. The uses of high pressure conditions [25], both chemical or physical water traps (dehydrating agents) [16, 26], and catalytic membrane reactors (CMR) [27] did not show a great improvement for the direct carboxylation reaction of methanol. Recently, Tomishige *et al.* first reported the use of 2-cyanopyridine (2-CP) as a dehydrating agent in the direct DMC formation from methanol and carbon dioxide in a batch system, demonstrating outstanding results in terms of methanol conversion and DMC selectivity (**Reaction 2**) as well as recycling of 2-picolinamide (2-PA) by dehydration reaction to 2-CP [28, 29]. Alongside the formation of DMC and 2-PA, very small amounts of methyl picolinate (Me-PCN) and methyl carbamate (Me-CBM) were reported as byproducts. The former is produced together with NH_3 as a result of the reaction between 2-PA and methanol (**Reaction 3**), while the latter is from the reaction between DMC and NH_3 (**Reaction 4**).

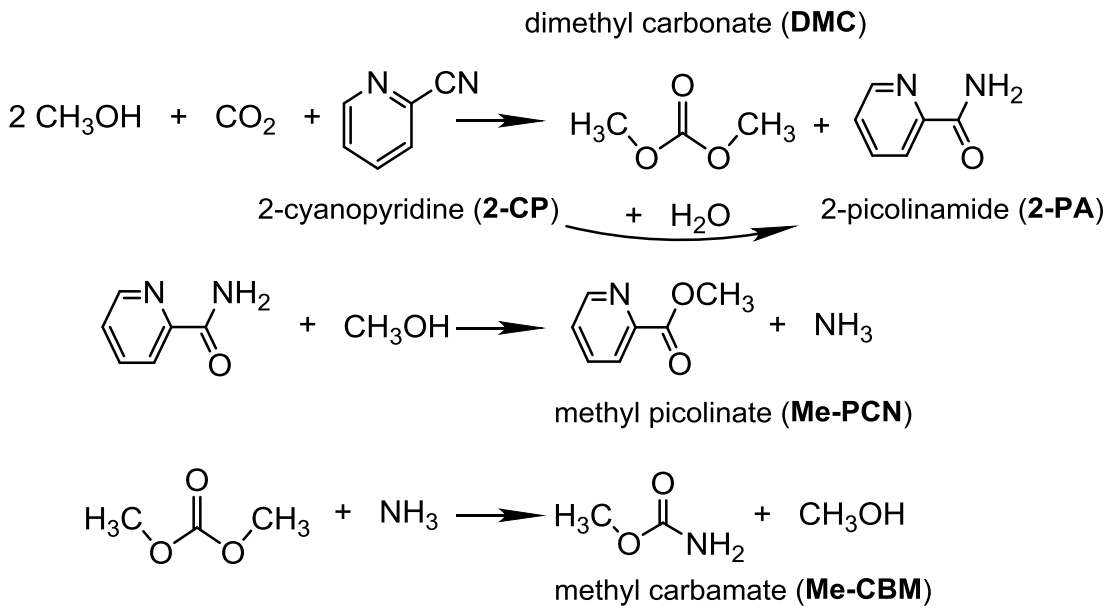

Inspired by the work of Tomishige, our group reported the direct DMC synthesis over ceria (CeO_2) catalysts in a fixed bed reactor in the presence of 2-CP with >90% methanol conversion and >95% DMC selectivity [25]. Very good results were obtained, but at the same time a drop in methanol conversion by ca. 50% was observed after ca. 200 h of continuous operation and the origin of the deactivation remains unclarified.

Operando methodology (*in situ* spectroscopy and simultaneous activity measurements under technically relevant catalytic reaction conditions) has been increasingly used over the last years for better understanding of catalytic materials and reaction mechanisms [30]. The use of traditional tubular quartz reactors as spectroscopic cells [31-36] is an extremely powerful and efficient approach given that a wide range of temperatures and pressures can be easily studied. On the other hand, visually inspecting catalysts in real time using such an optically transparent reactor can possibly offer new perspectives on catalytic reaction mechanism, catalyst functionality, and process optimization, often with the aid of *operando* spectroscopic probe(s). There are several reports where visual

observations were made on the basis of the use of quartz capillary reactors (or windows), such as working under high pressures (250 bar) and temperatures (500 °C) for biomass gasification [37], coke identification in the conversion of biomass in hot compressed water [38], assessment of the mixing behavior in a reformer prototype for hydrogen production [39], and evaluation of the temperature profile during the efficient reheating of a reverse-flow reformer [40].

The present study aims at first demonstrating the continuous DMC synthesis using CeO_2 as catalyst and 2-CP as dehydrating agent in a fused quartz reactor operated up to the optimum reaction pressure of 30 bar [25] and then at shedding light on critical parameters that can help better understand and improve the process by visual and spectroscopic inspections. Particular focuses are given to gain new insights into the origin of deactivation and its mechanism to propose effective conditions for catalyst reactivation. Furthermore, our first attempts to visualize the complexity of the catalytic interface consisting of three-phase boundaries (gas-liquid-solid) under *operando* conditions will be presented.

2. Experimental

2.1 Materials

High surface area CeO_2 powder (>100 m^2/g) was kindly supplied by Daiichi Kigenso Kagaku Kogyo Co. Ltd., Japan and used without any further treatment. Methanol (>99%) and 2-cyanopyridine (2-CP, 99%) were purchased from Sigma Aldrich. High purity CO_2 (>99.9993%) gas was purchased from Abelló Linde, Spain.

2.2 Reaction system

The details of the reaction set-up, protocols used, and analytical methods for the identification and quantification of reaction products were described in our previous work [25]. The reaction set-up used in this work is a simplified and improved version of the previously reported reaction system [25]. The present system differs in product separation efficiency by means of an improved hot trap design. This was achieved by introducing the hot trap into a home-made metallic oven. The temperature of the oven was kept at 130-140 °C so that high separation efficiency between low and high boiling-point compounds could be assured. The product analysis was performed by GC-MS (Scion 436-GC, Bruker) using ethanol as solvent and 1-hexanol as an internal standard. Additionally, n-octane was introduced in the reactant stream as an internal standard in order to minimize the errors in quantification of the products due to evaporation and condensation.

In a typical experiment, 300 mg of the CeO_2 catalyst (pelletized, crushed, and sieved to 200-300 µm particle size) was loaded into the reactor tube (fused quartz reactor with ID: 2.0 mm, and OD: 3.0 mm, purchased from Technical Glass Products, Inc. USA), resulting in the catalyst bed length of ca. 6.0 cm (Figure S1, Supplementary Information). The flow of CO_2 was kept at 6 NmL/min while the HPLC pump was operated at constant flow rate of 10 µL/min to pass the mixture of methanol and 2-CP at 2:1 molar ratio. The quartz reactor tube was connected to the reaction system using regular compression fittings, with the approach very similar to that described to achieve the high pressure sealing [41]. The compression fittings for quartz reactor included SS 316 nuts and Valcon polyimide ferrules (high temperature graphite-reinforced polyimide

composite), purchased from Swagelok® and Valco (VICI® AG International), respectively.

For the study of pressure and temperature effects, the reaction system was first stabilized for 2.5 h before starting the sample collection. Pressure effects on the reaction performance was examined from 1 to 30 bar at two temperatures (70 and 120 °C) by starting from 30 bar and step-by-step decreasing the pressure in the reactor. Temperature effects were investigated at 30 bar in the range of 80-160 °C. The first sample was collected at the lowest examined temperature of 80 °C and then the reaction at higher temperatures were studied. For all the cases (after switching from the initial conditions) 30 min of system stabilization and subsequent 45 min of sample collection period were applied.

2.3 Visual inspection and spectroscopic analysis

For the video recording of the catalyst under working conditions, the reactor furnace was modified by opening a channel of ca. 6 cm (long enough to see the whole catalyst bed) in the center of aluminum cover along the catalyst bed (Figure S2, Supplementary Information). This channel was covered by a glass window (above the aluminum cover) during the operation to minimize the heat loss while recording the catalyst under working conditions. The image/video recording was performed by two different video cameras: (i) a Panasonic Handy-Cam model SDR-S50 with a 78x enhanced optical zoom to record the overall picture of the furnace and quartz reactor and (ii) an USB

digital microscope (800-1000x magnification) – to obtain zoom-in images and videos at the level of the catalyst particles.

In situ and *operando* Raman measurements were performed with BWTEK dispersive i-Raman spectrometers equipped with 532 and 785 nm excitation lasers and a TE-cooled linear array detector. *Ex situ* Raman measurements were carried out on a Thermo Scientific™ Nicolet™ iS™50 FT-IR Spectrometer equipped with the Raman module with a 1064 nm near-infrared laser. FT-IR measurements were performed at 2 cm^{-1} resolution on a Bruker Alpha spectrometer equipped with a DTGS detector and a KBr beam splitter using a single-reflection ATR accessory with a diamond internal reflection element. Transmission FT-IR measurements were performed at 2 cm^{-1} resolution on an Agilent Technologies Cary 630 FTIR spectrometer equipped with a DTGS detector and a DialPath accessory with ZnSe windows at the path length of 100 μm.

Band assignments of IR and Raman spectra were assisted by quantum chemical calculations of vibrational frequencies and intensities and normal mode analysis. They were performed with density functional theory (DFT) using B3PW91 functional [42, 43] with 6-311G(2d,2p) basis sets using Gaussian 09 [44] as an isolated molecule without solvent effects. The simulated IR and Raman spectra are shown as the sum of Lorentzian lines taking the calculated IR/Raman intensity of a normal mode as the height at each vibrational frequency. The vibrational frequencies were empirically scaled by 0.98.

3. Results and discussion

3.1 Verification of fused quartz tubular reactor for continuous DMC synthesis

To test the capabilities of the fused quartz tube as a truly *operando* reactor, catalytic tests were performed and the catalytic results were evaluated under different reaction conditions. **Figure 1** shows the effects of reaction pressure on methanol conversion and product selectivity at 70 °C. As expected from the low reaction temperature, a very low methanol conversion was observed. Still, the use of the highly efficient dehydrating agent (2-CP) afforded 8% methanol conversion at 1 bar, much higher than the value observed at higher temperature at 400 bar without dehydrating agent (ca. 1%) [25]. The level of methanol conversion increased from 8.3% at 5 bar up to 12.4% at 30 bar. The DMC selectivity remained very high in the range of 96.3% (30 bar) – 98.2% (1 bar). The formation of the undesired side products (Me-PCN and Me-CBM, **Reactions 3 and 4**) increased at higher pressures. In fact, Me-CBM formation was only observed under the most DMC-productive condition (70 °C and 30 bar). This is likely a consequence of the enhanced NH_3 formation by increased Me-PCN selectivity (**Reaction 3**) from 1.8% (at 1 bar) to 2.7% (at 30 bar) as well as the enhanced DMC yield (at 30 bar) since both DMC and NH_3 required for Me-CBM formation (**Reaction 4**).

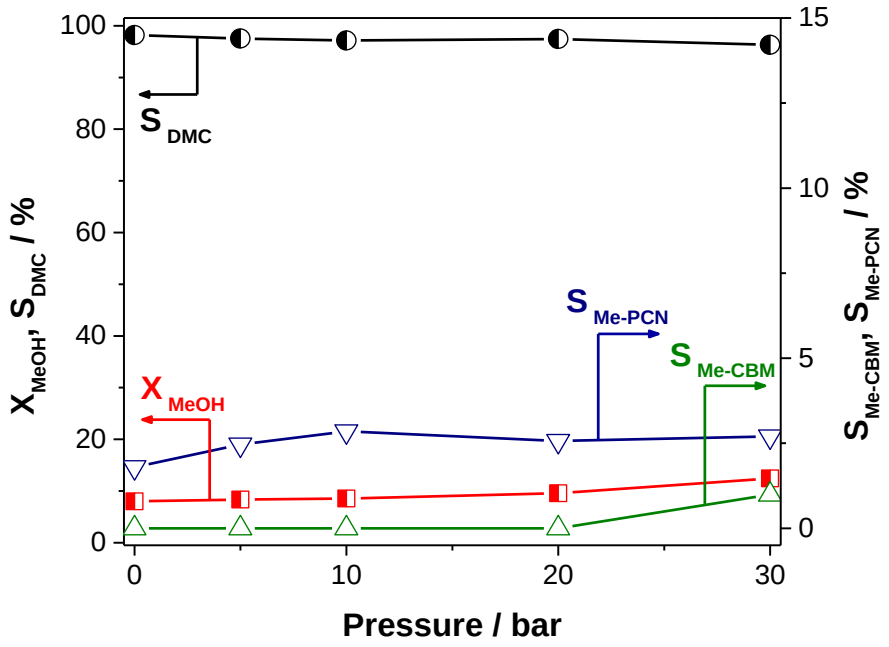

Figure 1. Effects of reaction pressure on methanol conversion (X_{MeOH}) and product selectivity (S_i: i = DMC, Me-PCN, Me-CBM) at 70 °C.

Figure 2 presents the effects of reaction pressure on methanol conversion and product selectivity at 120 °C. The methanol conversion follows the same profile as that reported in our previous study using a tubular reactor made of stainless steel [25]. The methanol conversion was strongly impacted by the increase in the reaction pressure. Even at 1 bar, 27.6% methanol conversion, more than three times higher compared to the value obtained at 70 °C, was observed. Increasing the pressure from 1 to 5 bar resulted in a drastic increase in methanol conversion (72.4%) and the prominent importance of 2-CP in the reaction was once again confirmed. Further increase in methanol conversion from 83.5% (10 bar), 88.6% (20 bar), to >92% (30 bar) was observed in good agreement with our previous work [25]. The increase in

reaction pressure resulted in an increase in DMC selectivity by suppressing the formation of by-products. At 1 bar the selectivity towards DMC was 91.2% (with more than 7% Me-PCN selectivity, and ca. 1.5% Me-CBM selectivity), while at 30 bar DMC was produced with >99% selectivity with high methanol conversion (92%). The positive influence of higher reaction pressure is ascribed to the suppression of NH_3 formation which is likely preferred at lower pressure conditions. When NH_3 formation is suppressed, both Me-PCN and Me-CBM formation will be minimized (*vide supra*).

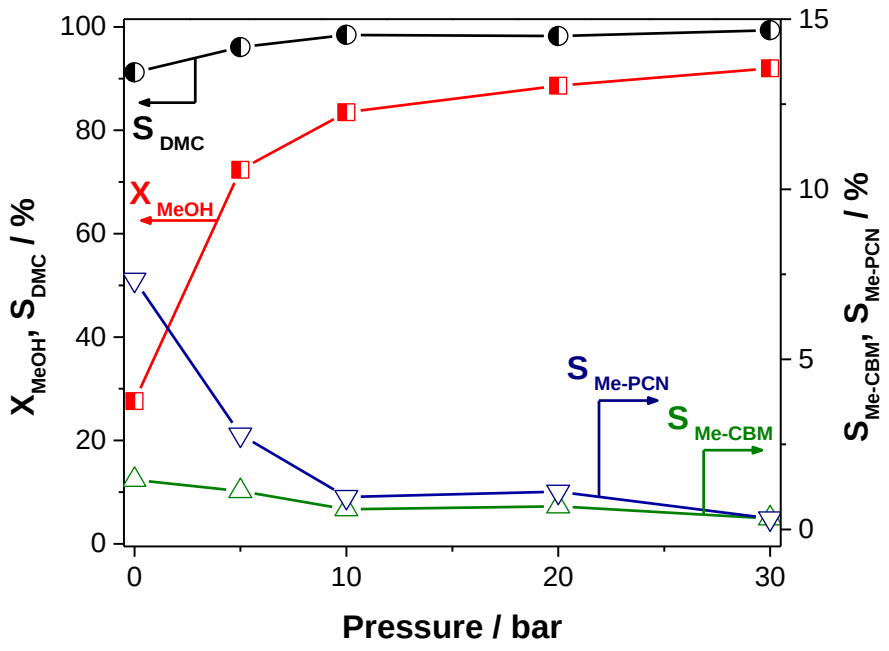

Figure 2. Effects of reaction pressure on methanol conversion (X_{MeOH}) and product selectivity (S_i: i = DMC, Me-PCN, Me-CBM) at 120 °C.

Figure 3 depicts the effects of reaction temperature on methanol conversion and product selectivity at 30 bar. At 80 °C, methanol conversion was low (17.6%) whereas high DMC selectivity (98.7%) was observed. DMC selectivity became very high and reached the maximum (>99%) at 120 °C. Above the temperature, both methanol conversion and DMC selectivity went down. On the contrary, the selectivity towards Me-PCN (3.2% at 140 °C, and 11.4% at 160 °C) and Me-CBM (1.8% at 140 °C, and 6.1% at 160 °C) greatly increased. These results indicate that **Reaction 3** and consequent NH_3 formation become more favorable at higher temperatures. This is most likely related to phase change of the reactants, especially methanol, which become gaseous above the temperature and therefore the suppression effects by the higher pressure conditions of **Reaction 3** as discussed above are less effective.

The above studies of the reaction temperature and pressure clearly assure that the catalytic reactor made of optically transparent fused quartz can be used as a routine laboratory reactor with the advantages of possible *operando* visual and spectroscopic inspections as described below.

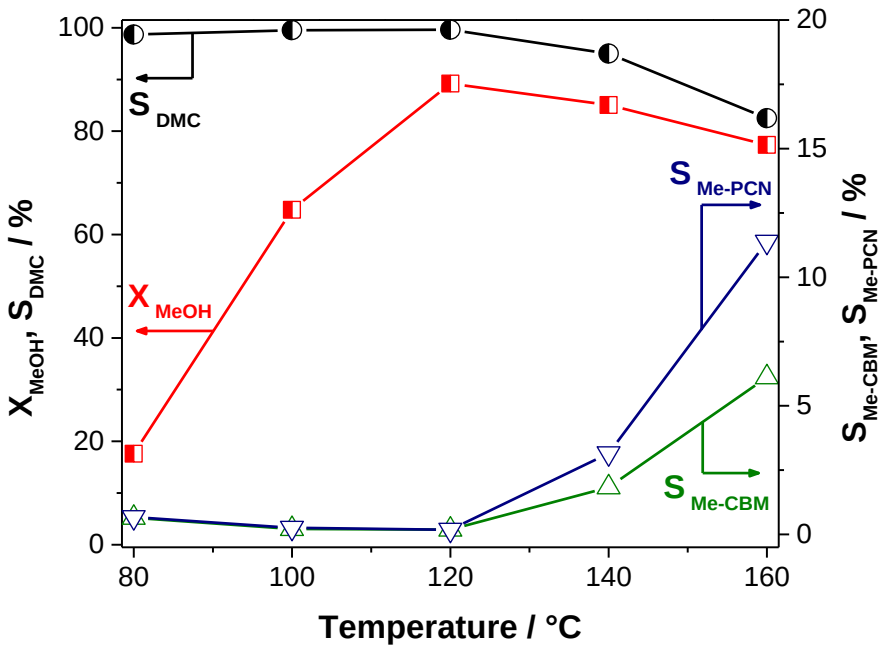

Figure 3. Effects of reaction temperature on methanol conversion (X_{MeOH}) and product selectivity (S_i: i = DMC, Me-PCN, Me-CBM) at 30 bar.

3.2 Catalyst deactivation-reactivation studies assisted by visual inspection

While the advantages of the heterogeneous catalysts over the homogeneous ones are widely recognized (e.g. in terms of product separation, re-use and scale up), one of the major problems that heterogeneous catalysts confront with is catalyst deactivation which becomes serious when the reaction scale is large. Even though the issue has not been clearly reported when the DMC synthesis was operated in the batch system (the catalyst was regenerated for three consecutive runs by calcination at 550 °C [28]), catalyst deactivation was confirmed when the reaction was run continuously [25].

The first striking observation that has drawn our attention during the catalytic tests using the fused quartz reactor was the color change of the ceria catalyst (from original light

yellow color to dark brown or even more blackened one) within the first hours of the reaction. **Figure 4** shows the catalysts after ca. 24 hours of reaction and subsequent drying in the furnace at 80 °C. Along with the color change, we could easily observe the formation of small crystallites that agglomerated and covered the surface of the catalyst.

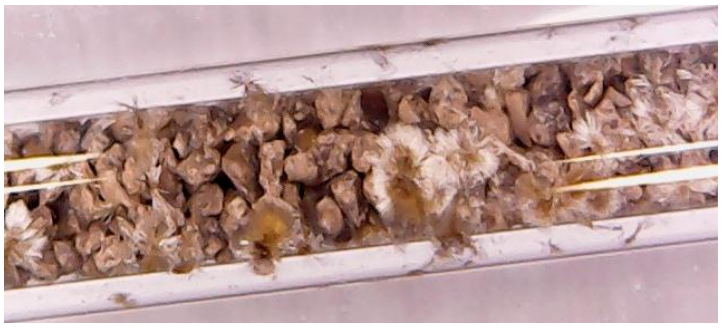

Figure 4. Photograph of the CeO_2 catalyst in the fused quartz reactor after 24 h of the reaction and subsequent drying.

The presence of a color gradient along the axial direction of the catalyst bed has to be noted as the color change was much more pronounced at the inlet of the reactor and less prominent towards the outlet (Figure S3, Supplementary Information). In addition, the color change was more accentuated when high methanol conversion was observed (Figure S3). We suspected that this color change of the catalyst and/or the formation of the substance (looks crystallites) covering the catalyst may be related to or cause the catalyst to deactivate over days of the reaction. Hence, some attempts were made to identify the origin of the catalyst deactivation and also an optimum condition for catalyst reactivation.

Our first attempt as a reactivation strategy was to wash the catalyst with the polar reactant, methanol. Initially, the washing was performed at room temperature under a

small methanol flow at 0.1-0.3 mL/min. Visually no drastic change could be observed with this mild washing condition, resulting in only with some surface cleaning of the accumulated crystallites (**Figure 5b**). As the next attempt, methanol was passed through the reactor at a higher flow rate (1-3 mL/min) at 120 °C. This treatment lightened the color of the catalyst remarkably after 30-60 min (**Figure 5c**).

Figure 5. Photograph of the CeO_2 catalyst at three different locations along the axial direction of the catalyst bed: **(a)** before the reaction, **(b)** after the DMC synthesis for 35 h and a short (5-10 s) methanol washing at room temperature to remove the majority of the crystallites covering the CeO_2 surface (Figure 4), **(c)** subsequent methanol washing at 120 °C for 1 h, and **(d)** after calcination of **(c)** under the flow of air at 300 °C for 12 h.

Encouraged by the great color change, catalytic tests were performed after methanol washing treatments at 120 °C and the catalytic activity expressed in terms of methanol conversion was compared with that without methanol washing (**Figure 6**). Without the methanol washing treatment, the activity dropped monotonously from 92.4% to ca. 70% in 70 h. To compare with this profile and check the influence of the washing treatment, the reaction was terminated after 20 h (**Figure 6**, run 1) and the catalyst was washed with methanol thoroughly for 4 h at 120 °C. Then the catalytic test was resumed for another 24 h (**Figure 6**, run 2). The catalytic activity was found to follow the trend of the unwashed catalyst. This procedure was repeated another time with increased washing time (40 h) and the reaction was tested for another 24 h (**Figure 6**, run 3). There was an apparent increase in methanol conversion after the second thorough washing but the increase was minor and followed the reaction profile of the unwashed catalyst. It is worth mentioning that the selectivity towards DMC was stably high (98-99%, not shown) during the catalytic tests after methanol-washing. On the other hand, in the catalytic test without methanol washing the DMC selectivity was slowly decreasing over 70 h of the reaction, reaching the final value around 90%. Even though the methanol washing protocol does help to keep the DMC selectivity stable over time, the catalyst deactivation (i.e. drop in methanol conversion) cannot be prevented by this protocol.

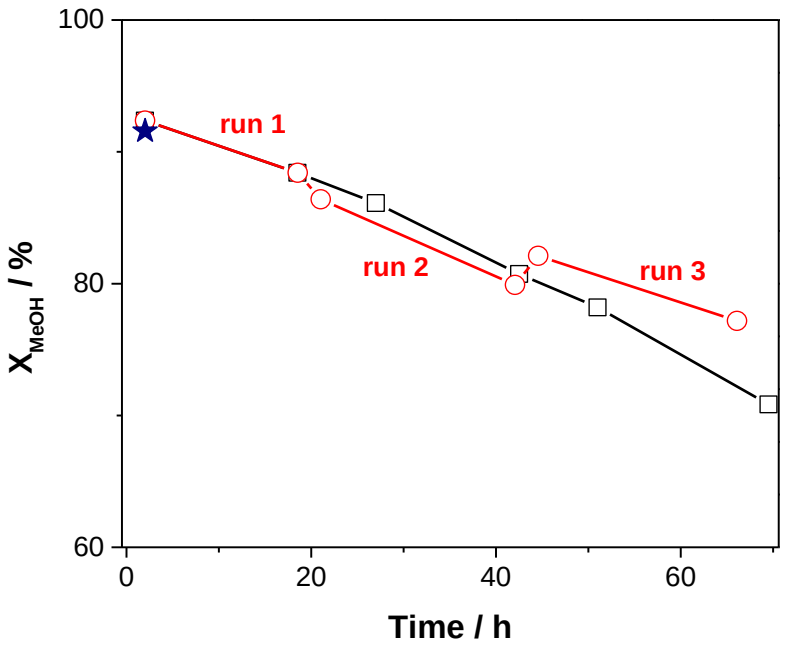

Figure 6. Deactivation-reactivation study using CeO_2 at 120 °C and 30 bar. Methanol conversion profile **a**) during a long-term catalytic test for 70 h (black line) and **b**) three consecutive catalytic runs (red lines) of ca. 20 h with methanol washing treatment between the runs (4 h washing between runs 1 and 2 and 40 h washing between runs 2 and 3, both at 120 °C). The blue star symbol shows the methanol conversion value after calcination of the methanol-washed catalyst at 300 °C.

Another strategy of catalyst reactivation by thermal treatment in air was evaluated since this is a general protocol for reactivation, especially to regain reactivity after coking. Thanks to the optically transparent fused quartz reactor, we monitored the color change during the thermal treatment (A video of the reaction process included in Supplementary Information). The catalyst material got slightly brighter when the temperature of the reactor was raised from 120 to 200 °C under air flow (20 mL/min). As soon as the

temperature approached ca. 280 °C the color of the catalyst turned lighter into more and more orange. It was just a matter of few seconds (while going from 280 to 290 °C) for the material to turn to light orange. The thermal treatment at 300 °C was sufficient to observe the material completely turning back to the yellowish color close to that of the original material (**Figure 5d**). Remarkably, the catalytic test of this material after the thermal treatment at 300 °C exhibited the identical performance as the original one (**Figure 6**) with methanol conversion (91.6%) and DMC selectivity (99.5%). This shows that the simple reactivation protocol under the relatively mild condition is sufficient for full recovery of the catalytic activity.

The textural properties (**Table S1** Supplementary Information) of i) the catalyst before the reaction, ii) catalysts after the reaction and washing, and iii) after the thermal treatment at 300 °C are in very good agreement with the visual observations and catalytic performance. The material after reaction and washing showed a drastic decrease in the BET surface area and pore volume, while they were recovered after the thermal treatment.

3.3 Spectroscopic investigation of the origin of catalyst deactivation

The use of optically transparent fused quartz reactor is ideal to perform spectroscopic studies, e.g. Raman and UV-Vis spectroscopy for which optical fiber-based spectrometer systems can be conveniently used. Therefore, besides visual inspection of the catalytic reactor, we have performed *operando* Raman study; however, it failed because of the compatibility of the excitation lasers of our mobile Raman systems (532 and 785 nm) with the target system to be studied. Under the reaction conditions, strong fluorescence was observed likely due to the products originating from 2-CP. This was

the case also after the thorough methanol washing. Therefore, we have investigated the catalyst materials in the reactor under different conditions (before/after the reaction, after methanol washing, and after air calcination) but *ex situ* using the Raman system equipped with a 1064 nm laser, with which the sample did not show fluorescence.

Figure 7a shows the Raman spectrum of the CeO_2 catalyst after the methanol washing. The spectral features are clearly defined, indicating that the species residing on the catalyst surface is not coke but a well-defined molecular entity. Also, the intensity due to the surface species increased towards the inlet of the catalyst bed, showing a larger accumulation of the surface species towards the front position as indicated by the darker color (**Figure 5c**). After comparing with the Raman spectra of different molecular references, we identified that the Raman spectrum resembles that of 2-PA (**Figure 7b**). The band assignments of 2-PA were made based on the previous reports for the molecule [45-49], the characteristic vibrational frequencies of the carboxamide group [46] and the DFT calculation (**Figure 7c** and normal mode analysis). **Table S2** (Supplementary Information) summarizes the observed Raman bands as well as the proposed assignments.

The 600–1800 cm^{-1} region of the Raman spectrum of 2-PA (**Figure 7b**) is dominated by the two very strong bands at 998 and 1587 cm^{-1} assigned to δ_{ring} and v_{ring} modes, respectively. Three significant bands observed at 782, 1167 and 1399 cm^{-1} are assigned to v_{ring}, $v(C_{ring}\text{-}C_{amide\ group})$, and Amide III (mainly v(C-N)) vibrations, respectively. The theoretical spectrum of 2-PA (**Figure 7c**) resembles the features of the experimental Raman spectrum of 2-PA with a few exceptions, e.g. the band at 1750 cm^{-1} (theory) corresponding to Amide I (mostly C=O stretching) which appears ca. 95

cm^{-1} red-shifted (experiment), the band at 1611 cm^{-1} (theory, corresponding to v_{ring}) which appears ca. 25 cm^{-1} red-shifted (experiment), and the band at 1363 cm^{-1} (theory, corresponding to Amide III) which appears ca. 35 cm^{-1} blue-shifted (experiment). These bands are mainly related to the vibrations of the amide functional group of 2-PA and they are likely shifted in the experimental spectrum because 2-PA molecules are packed in a form of crystallites within the sample via inter-molecular interactions via the amide group.

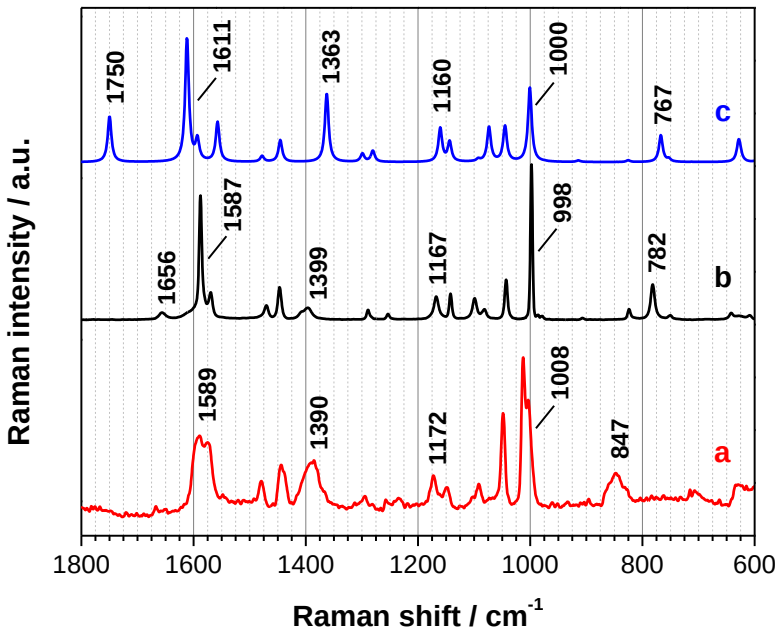

Figure 7. Raman spectra of **(a)** the CeO_2 catalyst after the reaction and subsequent methanol-washing treatment (Figure 5c) and after subtracting spectral contribution of CeO_2, **(b)** 2-PA powder, and **(c)** 2-PA calculated by the DFT method.

The Raman spectrum of the surface species over the methanol-washed CeO_2 after the reaction (**Figure 7a**) can be easily correlated with the bands of 2-PA (**Figures 7b and**

7c) with a few notable differences. The band at 847 cm^{-1} of the surface species appeared much more broadened and blue-shifted by 65 cm^{-1} compared to the band at 782 cm^{-1} of 2-PA. The band is assigned to the vibration involving a combined contribution of δ_{ring} and $v(C_{ring}\text{-}C_{amide\ group})$ [48]. Remarkably, the band corresponding to Amide I is hardly observable or red-shifted to the extent that merged with the band at ca. 1590 cm^{-1}. The great shifts of the two bands indicate that 2-PA is adsorbed on the surface via the amide group.

A very similar shift of the first band (combined δ_{ring} and $v(C_{ring}\text{-}C_{amide\ group})$) was observed in the SERS spectra of benzamide [50, 51] and 2-PA [45, 49], undergoing a blue-shift of the same magnitude with respect to the Raman band of the solids of the respective molecule (53 and 48 cm^{-1}, respectively). The observed blue-shift has been attributed by Otero and co-workers [49, 51] to the adsorption of benzamide or 2-PA molecule on a metal surface in its azanion ($Ar\text{-}CONH^-/Py\text{-}CONH^-$, Ar = aryl and Py = pyridyl ring) form, that is, with the carboxamide group partially deprotonated. While the formation of the azanion goes via deprotonation of the tautomeric carboxamide and carboximidic forms of the corresponding amides (**Scheme 1**), the high stability of the deprotonated amide could be due to electron delocalization along the π–system of the functional group and the pyridyl ring.

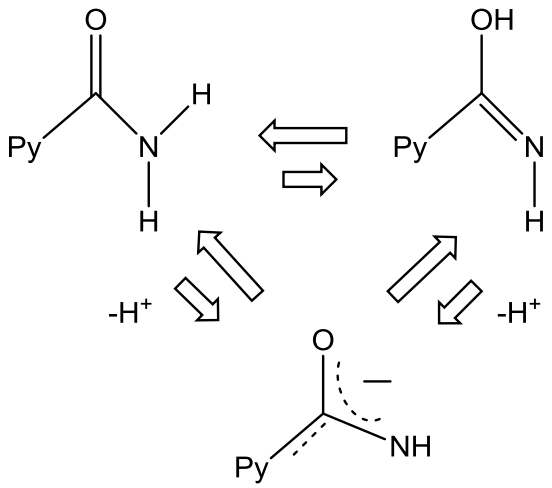

Scheme 1. Formation of the azanion by deprotonation of the tautomeric carboxamide and carboximidic forms of 2-PA [49].

Furthermore, **Figure 8** shows a similar study by IR spectroscopy. For the IR study, the 2-PA spectrum was measured in transmission mode in a diluted form in an apolar solvent (toluene) to minimize the intermolecular interactions which were observed for the solid sample (not shown). The IR spectrum of the catalyst after the methanol washing was recorded by removing the sample from the reactor and in the ATR sampling configuration to minimize light absorption by CeO_2 and to maximize signals from surface species. The band assignments of 2-PA are based on those previously proposed for this molecule [47, 48, 52, 53] as well as by the DFT calculation. **Table S3** (Supplementary Information) summarizes the observed IR bands as well as the proposed assignments.

The 600–1800 cm^{-1} region of the IR spectrum of 2-PA (**Figure 8b**) is dominated by four important features at 750, 1368, 1557, and 1700 cm^{-1} assigned to δ_{ring}, ν(C-N), δ(NH_2),

and v(C=O) modes, respectively. The theoretical IR spectrum of 2-PA (**Figure 8c**) is in good agreement with the experimental one (**Figure 8b**) except the band at 1750 cm^{-1} which corresponds to v(C=O), indicating that the vibrational mode is still, upon dilution in toluene, mildly interacting intermolecularly via the N-H group of the amide group.

The IR spectrum of the surface species on CeO_2 after the reaction (**Figure 8a**) can be again correlated with the characteristic bands of 2-PA (**Figures 8b and 8c**). The notable difference is the absence or rather likely a significant red-shift of the v(C=O) mode. Furthermore, two broad bands at ca. 1393 and ca. 1562 cm^{-1} are observed. The broadness of the bands as well as the suspected large red-shift of v(C=O) bands indicate that the surface species (likely 2-PA) interact with the heterogeneous structure of the CeO_2 surface via the amide group in a flexible manner or via various configurations of adsorption. According to literature, the existence of the CON functional group and the formation of 2-PA monoanion ($Py\text{-}CONH^-$) on CeO_2 surface can be suggested [54-60]. Moreover, no trace of nitrile group (-CN, characteristic absorption around 2200-2300 cm^{-1}) was observed on the IR spectrum of CeO_2 after the reaction and washing. This clearly indicates that not 2-CP but 2-PA-like species are responsible for poisoning the catalyst by strongly binding over the active sites of the CeO_2 surface.

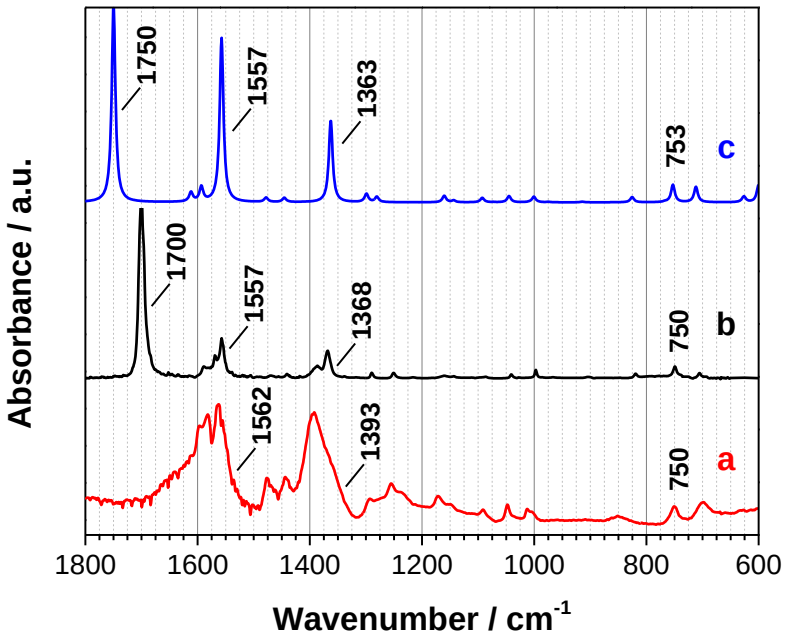

Figure 8. IR spectra of **(a)** the CeO_2 catalyst after the reaction and subsequent the methanol-washing treatment (Figure 5c) and after subtracting spectral contribution of CeO_2, **(b)** 0.1 M 2-PA in toluene (toluene contribution subtracted), and **(c)** 2-PA calculated by the DFT method.

In the direct DMC synthesis from CO_2 and methanol in the presence of 2-CP in a batch system, Tomishige *et al.* reported that the presence of an effective nitrile will lead, upon hydration, to amides that can weakly adsorb on CeO_2 surface via intramolecular H bonding and also that they can easily desorb from the surface, thereby not causing catalyst poisoning [28, 29]. At the same time, mechanistic studies of the nitriles hydration to amides over CeO_2 catalysts confirm the presence of an amide anion intermediate (**Scheme 2b**) [29] which was resulted via the interaction of both N and O atoms of this ionized amide group with the surface Ce atom as the key step of the

reaction [60]. This intermediate is similar to the species indicated by the Raman and IR studies and likely causing deactivation.

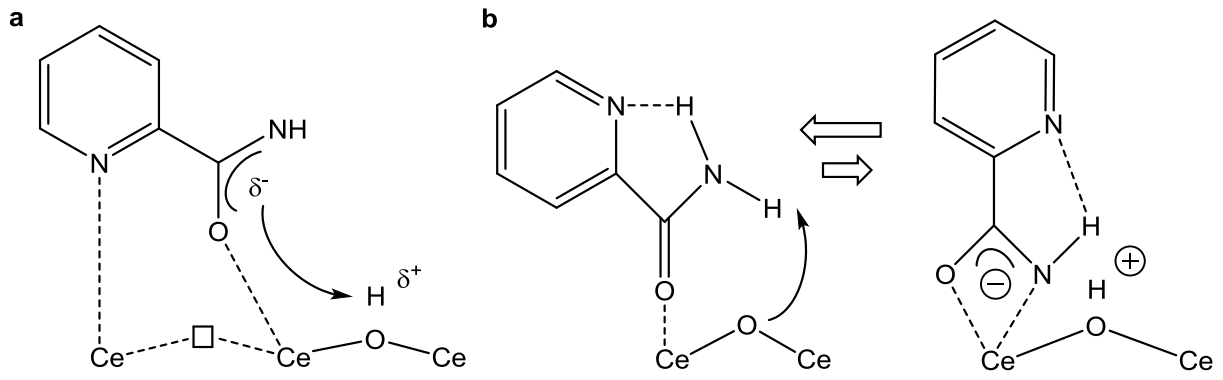

Scheme 2. (**a**) A proposed mechanism for nitrile hydration on CeO_2 going via the amide anion intermediate (adapted from [60] with permission from The Royal Society of Chemistry) and (**b**) the suggested adsorption state of 2-PA in direct DMC synthesis from CO_2 and methanol in the presence of 2-CP (adapted from [29] with permission from Elsevier).

The visual inspection (**Figure 5**) and catalyst reactivation study (**Figure 6**) indicated that the reactivation takes place, judging from the color change, in the temperature interval between 280-290 °C and completes below 300 °C. Very interestingly, this temperature matches with the boiling point of 2-PA (284.1 °C at 760 mmHg; **Table S4** in Supplementary Information summarizes the melting and boiling points of the 2-CP-derived chemicals). Taking the Raman and IR spectroscopic results into account, we attribute that 2-PA is adsorbed via the amide group over CeO_2 and it causes the catalyst to deactivate.

3.4 Operando visual inspection

Using the fused quartz reactor, we have finally attempted to shed light on the catalyst surface under *operando* conditions where gas (CO_2 and methanol) and liquid (2-CP and 2-PA) are mixed over the catalyst surface at the optimum temperature (120 °C). According to our previous study, the residence time of the reactants was roughly estimated to be ca. 20 s at 30 bar [25]. It is of great interest and importance to gain how the catalytic interface of the three-phase boundary looks like to gain insights into the mass transfer and key factors enabling the high methanol conversion and DMC selectivity within such a short residence time in comparison to the batch reaction cases (in the order of hours).

Occasional traveling of liquid droplets through the catalyst bed could be observed at 70 °C (not shown), but this was not the case at 120 °C. Although at first glance the catalyst under the optimum condition (30 bar, 120 °C) looked dry, a closer look at the magnified level of the catalyst particle clarified that the surface of the catalyst was constantly wet (A video under representative condition is shown in Supplementary Information). This indicates that 2-CP, 2-PA and possibly methanol cover the CeO_2 catalyst as liquid and CO_2 gets dissolved into the liquid to get in contact with the reactants as well as the catalyst surface for the reaction to take place. Also, there was a formation of white islands (likely the crystallites of 2-PA) growing with time over the catalyst surface. The color of the islands and coating changed darker upon drying and this was the coating removed by hot-methanol washing as described above. Apparently, the surface became more dry at lower pressure conditions (**Figure 9**) probably due to the higher actual flow rate of gas phase CO_2 and methanol at lower pressures, which facilitated the removal of the liquid phase coating over the catalyst surface. This could positively impact on the

reaction performance by improving the contact of CO_2 with the reactants and with the catalyst surface, but it was not the case and higher pressure conditions (where the catalyst surface was more wet) were favorable for the catalytic performance (**Figure 2**). Longer residence time at higher pressure conditions may have also contributed to the enhanced catalytic performance.

The catalyst deactivated but not completely after some days of the reaction. This implies that the active sites of the catalyst are still accessible when the catalyst surface is covered by the coating of some crystallites. The visual inspection has elucidated the accessibility of the bulk region of the catalyst particle. The video (Supporting Information) shows that when liquid droplets (mainly products and 2-PA) travels back through the reactor upon a sudden set-pressure decrease, the whole catalyst particle gets soaked by the droplets as evidenced by the color change. This clearly indicates the porosity and accessibility of catalytic sites in the bulk, thus maintaining the catalytic activity over some days of operation without full deactivation by the surface coating with the crystallites.

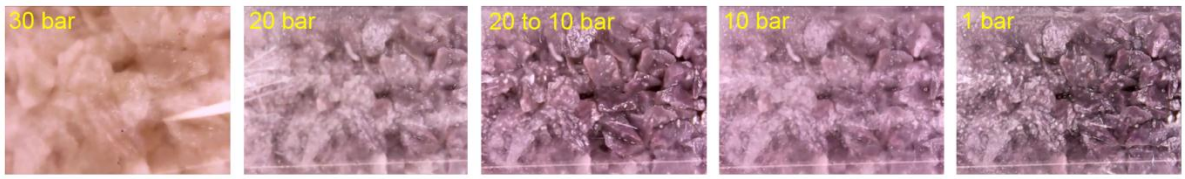

Figure 9. *Operando* visualization of the CeO_2 catalyst during the DMC synthesis from CO_2 and methanol in the presence of 2-CP. The experiment was started under the optimized reaction condition (30 bar, 120 °C) and subsequently the reaction pressure

was lowered. The darker color at lower pressures is caused by the time-sequence of the experiment.

4. Conclusions

The present study shows a successful demonstration on how one can employ fused quartz reactors to gain unique insights into the continuous dimethyl carbonate (DMC) synthesis from carbon dioxide and methanol over CeO_2 catalysts in the presence of a dehydrating agent (2-cyanopyridine). The catalytic performance was identical to that using a conventional stainless steel reactor. The fused quartz reactor can offer new perspectives on the catalytic process and its design by the verified concept that a picture is worth a thousand words (or numerous experiments without seeing inside). It allowed visual inspection of the catalyst under working conditions and observing drastic color change of the ceria materials (from light yellow to dark maroon) even within the first few hours of reaction. These observations were correlated with the lowered methanol conversion values. Based on the Raman and IR studies, it was identified that not coke but 2-picolinamide is the main source of catalyst deactivation by strongly binding to and thus poisoning the catalyst surface. The *ex situ* space resolved spectroscopic studies along the catalyst bed revealed the existence of a concentrational gradient of adsorbed surface species, reflecting how much the catalyst was poisoned (more intense towards the inlet and less intense towards the outlet of the reactor) in good agreement with the color gradient visually observed. Complete catalyst reactivation was achieved under mild conditions, just by using *in situ* methanol washing coupled with a moderate thermal treatment at the temperature slightly above the boiling

point of 2-picolinamide. Moreover, the use of quartz reactors afforded the observation of the complete synergy between the solid catalyst, the liquid methanol and 2-cyanopyridine mixture, and gaseous CO_2 – the reaction is taking place in both bulk and surface of CeO_2 catalyst. This study opens new opportunities in heterogeneous catalysis on how to investigate continuous processes which involve deactivation and take place at three-phase boundaries and on how to take advantage of the visual observations for better understanding and optimization of heterogeneously catalyzed reactions.

Acknowledgements

We acknowledge MINECO for financial support (CTQ2012-34153) and for support through Severo Ochoa Excellence Accreditation 2014-2018 (SEV-2013-0319). Recognition from the Catalan government (2014 SGR 893) is kindly acknowledged.

References

[1] P. Friedlingstein, R.A. Houghton, G. Marland, J. Hackler, T.A. Boden, T.J. Conway, J.G. Canadell, M.R. Raupach, P. Ciais, C. Le Quéré, Nat. Geosci., 3 (2010) 811–812.
[2] T.M. Gerlach, Eos, Trans. Amer. Geophys. Union, 92 (2011) 201-202.
[3] A. Bansode, A. Urakawa, J. Catal., 309 (2014) 66–70.
[4] Y. Ono, Appl. Catal. A-Gen., 155 (1997) 133–166.
[5] A.-A.G. Shaikh, S. Sivaram, Chem. Rev., 96 (1996) 951–976.
[6] N. Keller, G. Rebmann, V. Keller, J. Mol. Catal. A-Chem., 317 (2010) 1-18.
[7] D. Delledonne, F. Rivetti, U. Romano, Appl. Catal. A-Gen., 221 (2001) 241–251.
[8] M. Aresta, E. Quaranta, ChemTech, 27 (1997) 32-40.
[9] T. Sakakura, J.-C. Choi, H. Yasuda, Chem. Rev., 107 (2007) 2365–2387.
[10] M.A. Pacheco, C.L. Marshall, Energ. Fuel., 11 (1997) 2–29.
[11] K. Tomishige, T. Sakaihori, Y. Ikeda, K. Fujimoto, Catal. Lett., 58 (1999) 225-229.
[12] K. Tomishige, Y. Ikeda, T. Sakaihori, K. Fujimoto, J. Catal., 192 (2000) 355–362.
[13] Y. Ikeda, T. Sakaihori, K. Tomishige, K. Fujimoto, Catal. Lett., 66 (2000) 59-62.
[14] Y. Ikeda, M. Asadullah, K. Fujimoto, K. Tomishige, J. Phys. Chem. B, 105 (2001) 10653–10658.
[15] K. Tomishige, Y. Furusawa, Y. Ikeda, M. Asadullah, K. Fujimoto, Catal. Lett., 76 (2001) 71-74.

[16] K. Tomishige, K. Kunimori, Appl. Catal. A-Gen., 237 (2002) 103–109.
[17] H.J. Hofmann, A. Brandner, P. Claus, Chem. Eng. Technol., 35 (2012) 2140–2146.
[18] Y. Yoshida, Y. Arai, S. Kado, K. Kunimori, K. Tomishige, Catal. Today, 115 (2006) 95–101.
[19] M. Aresta, A. Dibenedetto, C. Pastore, C. Cuocci, B. Aresta, S. Cometa, E.D. Giglio, Catal. Today, 137 (2008) 125–131.
[20] M. Aresta, A. Dibenedetto, C. Pastore, A. Angelini, B. Aresta, I. Pápai, J. Catal., 269 (2010) 44–52.
[21] X.L. Wu, M. Xiao, Y.Z. Meng, Y.X. Lu, J. Mol. Catal. A-Chem., 238 (2005) 158–162.
[22] X.L. Wu, Y.Z. Meng, M. Xiao, Y.X. Lu, J. Mol. Catal. A-Chem., 249 (2006) 93–97.
[23] B.A.V. Santos, V.M.T.M. Silva, J.M. Loureiro, D. Barbosa, A.E. Rodrigues, Fluid Phase Equilibr., 336 (2012) 41–51.
[24] B.A.V. Santos, C.S.M. Pereira, V.M.T.M. Silva, J.M. Loureiro, A.E. Rodrigues, Appl. Catal. A-Gen., 455 (2013) 219–226.
[25] A. Bansode, A. Urakawa, ACS Catal., 4 (2014) 3877–3880.
[26] B.A.V. Santos, V.M.T.M. Silva, J.M. Loureiro, A.E. Rodrigues, Ind. Eng. Chem. Res., 53 (2014) 2473–2483.
[27] C.-F. Li, S.-H. Zhong, Catal. Today, 82 (2003) 83–90.
[28] M. Honda, M. Tamura, Y. Nakagawa, S. Sonehara, K. Suzuki, K.-i. Fujimoto, K. Tomishige, ChemSusChem, 6 (2013) 1341–1344.
[29] M. Honda, M. Tamura, Y. Nakagawa, K. Nakao, K. Suzuki, K. Tomishige, J. Catal., 318 (2014) 95–107.
[30] M.A. Bañares, Catal. Today, 100 (2005) 71-77.
[31] S.J. Tinnemans, J.G. Mesu, K. Kervinen, T. Visser, T.A. Nijhuis, A.M. Beale, D.E. Keller, A.M.J.v.d. Eerden, B.M. Weckhuysen, Catal. Today, 113 (2006) 3-15.
[32] T.A.X. Nijhuis, S.J. Tinnemans, T. Visser, B.M. Weckhuysen, Phys. Chem. Chem. Phys., 5 (2003) 4361-4365.
[33] J.W. Couves, J.M. Thomas, D. Waller, R.H. Jones, A.J. Dent, G.E. Derbyshire, G.N. Greaves, Nature, 354 (1991) 465-468.
[34] A.M. Beale, A.M.J.v.d. Eerden, K. Kervinen, M.A. Newton, B.M. Weckhuysen, Chem. Commun., (2005) 3015-3017.
[35] A. Brückner, E. Kondratenko, Catal. Today, 113 (2006) 16–24.
[36] M.G. O'Brien, A.M. Beale, S.D.M. Jacques, M.D. Michiel, B.M. Weckhuysen, ChemCatChem Catalysis, 1 (2009) 99 - 102.
[37] B. Potic, S.R.A. Kersten, M. Ye, M.A.v.d. Hoef, J.A.M. Kuipers, W.P.M.v. Swaaij, Chem. Eng. Sci., 60 (2005) 5982 – 5990.
[38] B. Potic, S.R.A. Kersten, W. Prins, W.P.M.v. Swaaij, Ind. Eng. Chem. Res., 43 (2004) 4580-4584.
[39] C. Tellaeche, B. Glöckler, G. Kolios, U. Nieken, Chem. Eng. Technol., 32 (2009) 1348–1357.
[40] B. Glöckler, H. Dieter, G. Eigenberger, U. Nieken, Chem. Eng. Sci., 62 (2007) 5638 – 5643.
[41] A. Bansode, G. Guilera, V. Cuartero, L. Simonelli, M. Avila, A. Urakawa, Rev. Sci. Instrum., 85 (2014) 084105
[42] A.D. Becke, J. Chem. Phys., 98 (1993) 5648–5652.
[43] J.P. Perdew, Y. Wang, Phys. Rev. B, 45 (1992) 13244–13249.
[44] M.J. Frisch, G.W. Trucks, H.B. Schlegel, G.E. Scuseria, M.A. Robb, J.R. Cheeseman, G. Scalmani, V. Barone, B. Mennucci, G.A. Petersson, H. Nakatsuji, M. Caricato, X. Li, H.P. Hratchian, A.F. Izmaylov, J. Bloino, G. Zheng, J.L. Sonnenberg, M. Hada, M. Ehara, K. Toyota, R. Fukuda, J. Hasegawa, M. Ishida, T. Nakajima, Y. Honda, O. Kitao, H. Nakai, T. Vreven, J. Montgomery, J. A., J.E. Peralta, F. Ogliaro, M. Bearpark, J.J. Heyd, E. Brothers, K.N. Kudin, V.N. Staroverov, R. Kobayashi, J. Normand, K. Raghavachari, A. Rendell, J.C. Burant, S.S. Iyengar, J. Tomasi, M. Cossi, N. Rega, J.M. Millam, M. Klene, J.E. Knox, J.B. Cross, V. Bakken, C. Adamo, J. Jaramillo, R.

Gomperts, R.E. Stratmann, O. Yazyev, A.J. Austin, R. Cammi, C. Pomelli, J.W. Ochterski, R.L. Martin, K. Morokuma, V.G. Zakrzewski, G.A. Voth, P. Salvador, J.J. Dannenberg, S. Dapprich, A.D. Daniels, O. Farkas, J.B. Foresman, J.V. Ortiz, J. Cioslowski, D.J. Fox, Gaussian 09, Revision A.02, Gaussian, Inc., Wallingford CT, 2009.

[45] J.F. Arenas, M.A. Montanez, J.C. Otero, J.I. Marcos, J. Mol. Struct., 293 (1993) 341-344.

[46] N.P.G. Roeges, A Guide to the Complete Interpretation of Infrared Spectral of Organic Structures, Wiley1994.

[47] E. Akalin, S. Akyuz, Vib. Spectrosc., 42 (2006) 333–340.

[48] M. Bakiler, O. Bolukbasi, A. Yilmaz, J. Mol. Struct., 826 (2007) 6-16.

[49] J.L. Castro, J.F. Arenas, M.R. Lopez-Ramirez, J. Soto, J.C. Otero, J. Colloid. Interf. Sci., 396 (2013) 95–100.

[50] J.F. Arenas, J.L. Castro, J.C. Otero, J.I. Marcos, J. Raman Spectrosc., 23 (1992) 249-252.

[51] J.L. Castro, M.R. Lopez-Ramirez, J.F. Arenas, J. Soto, J.C. Otero, Langmuir, 28 (2012) 8926−8932.

[52] S. Akyuz, T. Akyuz, Vib. Spectrosc., 42 (2006) 387–391.

[53] A. Borba, A. Gomez-Zavaglia, R. Fausto, J. Phys. Chem. A, 112 (2008) 45-57.

[54] H. Krietenbrink, H. Knözinger, Z. Phys. Chem., 102 (1976) 43-56.

[55] D.K. Paul, S.D. Worley, J. Phys. Chem., 94 (1990) 8956–8959.

[56] A. Aboulayt, C. Binet, J.-C. Lavalley, J. Chem. Soc., Faraday Trans., 91 (1995) 2913-2920.

[57] W.-C. Wu, L.-F. Liao, C.-C. Chuang, J.-L. Lin, J. Catal., 195 (2000) 416–419.

[58] C.-C. Chuang, W.-C. Wu, M.-X. Leea, J.-L. Lin, Phys. Chem. Chem. Phys., 2 (2000) 3877-3882.

[59] L.-F. Liao, C.-F. Lien, D.-L. Shieh, F.-C. Chen, J.-L. Lin, Phys. Chem. Chem. Phys., 4 (2002) 4584–4589.

[60] M. Tamura, A. Satsuma, K.-i. Shimizu, Catal. Sci. Technol., 3 (2013) 1386-1393.

Supplementary Information

Catalysis under microscope: Unraveling the mechanism of catalyst de- and re-activation in the continuous dimethyl carbonate synthesis from CO_2 and methanol in the presence of a dehydrating agent

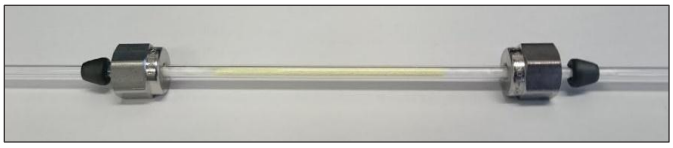

Figure S4. Fused quartz reactor with regular compression fittings. Fresh CeO_2 catalyst is loaded inside the reactor.

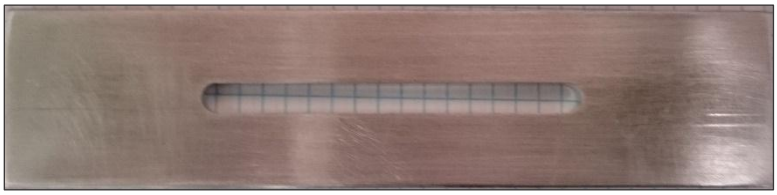

Figure S5. Home-made Aluminum cover plate for the reactor furnace with ca. 6 cm channeling to allow the visual recording of the experiments.

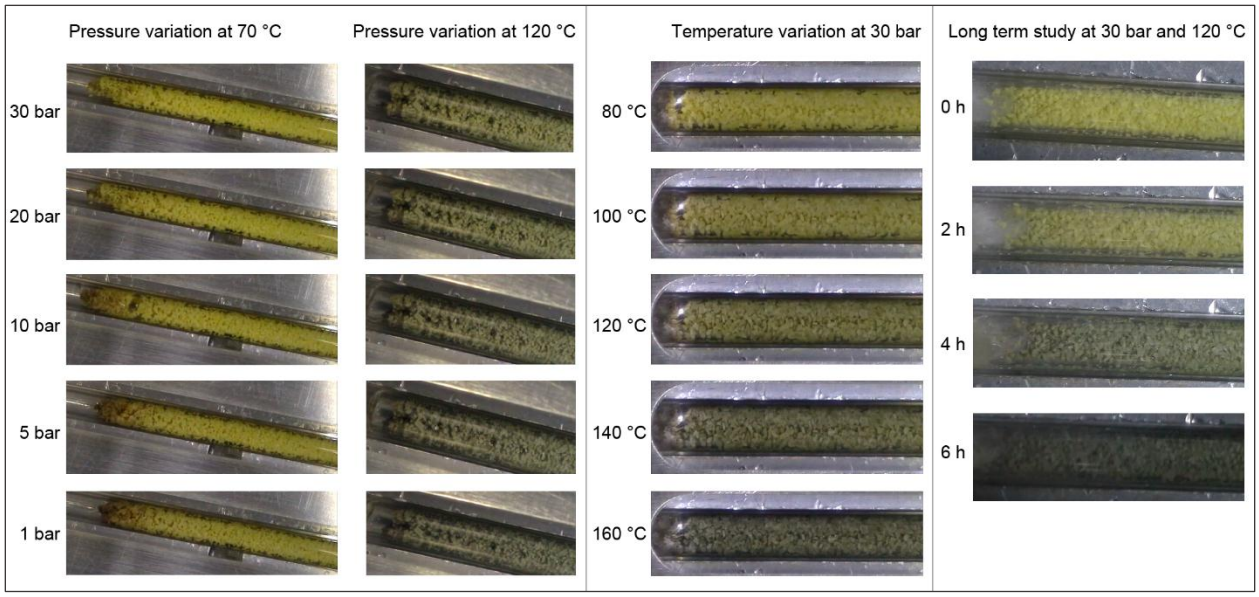

Figure S3. Color change of CeO_2 during the DMC synthesis. Snapshots of the catalyst bed close to the inlet of the reactor taken during the verification of the performance of the fused quartz reactors with the Panasonic handy-cam.

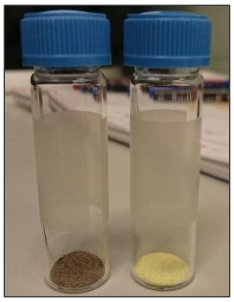

Figure S6. CeO_2 after reaction and washing (left) and after thermal treatment (right).

Table S1. BET surface area and pore volume of the CeO_2 catalyst i) before the reaction, ii) after the reaction and washing, and iii) after calcination. Two different batches/experiments are presented for comparison purposes.

Property / material	CeO_2 (initial)	after reaction and washing (batch 1)	after reaction and washing (batch 2)	after calcination (batch 1)	after calcination (batch 2)
S_{BET} (m^2/g)	150	108	119	141	130
Pore volume (cc/g)	0.197	0.135	0.148	0.146	0.156

Table S2. Raman band assignments of 2-picolinamide (solid reference), surface species on ceria after the reaction and methanol washing (after subtracting pristine ceria spectrum), and theoretical (DFT) vibrational frequencies of 2-picolinamide. ***** ν - stretching, δ - in-plane bending, γ - out-of-plane bending, ρ - rocking, sh. – shoulder, **~** – hardly identifiable. The notion of assignments is in accordance with ref [1].

2-PA solid	**Surface species on CeO_2 after methanol washing**	**2-PA (DFT)**	**Assignments***
1656	1658 (~)	1750	Amide I
1587	1589	1611 (sh.1593)	8a; ν_{ring}
1569	1574 (~)	1557	8b; ν_{ring}
1470	1479	1478	19a; ν_{ring}
1447	1444	1445	19b; ν_{ring}
1399	1390	1363	Amide III
1289	1295	1299	3; δ(CH)

1254	1245	1280	14; v_{ring}
1167	1172	1160	13; v(C-X)
1142	1148	1143	9a; δ(CH)
1099	1102 (~)	1092 (?)	15; δ(CH)
1081	1091	1073	ρ(NH_2)
1043	1048	1045	18a; δ(CH)
998	1008	1000	12; δ_{ring}
824	-	826	10a; γ(CH)
782	847	767	1; v_{ring}
750	715 (~)	753 (sh.)	10b; γ(CH)
642	634 (~)	628	6b; δ_{ring}

Table S3. IR bands assignments for 2-picolinamide (0.1 M in toluene), surface species on ceria after the reaction and methanol washing (after subtracting pristine ceria spectrum), and theoretical (DFT) vibrational frequencies of 2-picolinamide. ***** v - stretching, δ - in-plane bending, γ - out-of-plane bending.

2-PA liquid	**2-PA on CeO_2**	**2-PA (DFT)**	**Assignments***
1700	–	1750	v(C=O) – Amide I
1590	1597	1612	v_{ring}
1569	1582	1593	v_{ring}
1557	*1562*	1557	δ(NH_2) – Amide II
–	1476	1478	v_{ring} + δ(CH)
–	1443	1445	v_{ring}
1386, 1368	*1393*	1363	v(C-N) – Amide III
1289	1293	1299	δ(CH)
1250	1254	1280	v_{ring}
1160	1170	1160	v_{ring}
1042	1046	1044	δ_{ring}
998	1007	1001	δ_{ring}
820	849	825	γ(C=O)
750	750	753	δ_{ring}
705	700	711	γ(CH)

Table S4. Physical properties of the heavier compounds involved in the DMC synthesis from CO_2 and methanol in the presence of a dehydrating agent (r.t. = room temperature). Entries 4-6 (presenting similar chemical structures) are shown as relevant reference information due to the lack of solid data for methyl picolinate boiling point at ambient temperature and pressure [2].

Compound	Melting point (°C)	Boiling point (°C)
2-cyanopyridine	24-27	212-215
methyl carbamate	56-58	176-177
methyl picolinate	liquid / r.t.	95 / 1 mmHg
methyl nicotinate	42-44	204
methyl isonicotinate	liquid / r.t.	207-209
ethyl-2-picolinate	liquid / r.t.	240-241
2-picolinamide	110	284.1

References

[1] J.L. Castro, J.F. Arenas, M.R. Lopez-Ramirez, J. Soto, J.C. Otero, J. Colloid. Interf. Sci., 396 (2013) 95–100.

[2] http://www.sigmaaldrich.com/, Sigma-Aldrich Co. LLC., 2015.